Earth and Planetary Science Letters 552 (2020) 116595

Contents lists available at ScienceDirect

Earth and Planetary Science Letters

www.elsevier.com/locate/epsl

Lightning-induced weathering of Cascadian volcanic peaks

Jonathan M. Castro [a,*], Franziska Keller [b], Yves Feisel [a], Pierre Lanari [c], Christoph Helo [a], Sebastian P. Mueller [d], C. Ian Schipper [e], Chad Thomas [f]

[a] Institute of Geosciences, Johannes Gutenberg University, Mainz, Germany
[b] Department of Earth Sciences, ETH, Sonneggstr. 5, 8092 Zürich, Switzerland
[c] Institute of Geology, University of Bern, Baltzerstr. 3, 3012 Bern, Switzerland
[d] Department of Geography, Philipps-University Marburg, Deutschhausstr. 10, D-35037, Germany
[e] School of Geography, Environment and Earth Sciences, Victoria University, P.O. Box 600, Wellington 6140, New Zealand
[f] Chevron, 6001 Bollinger Canyon Road, San Ramon, CA 94583, USA

ARTICLE INFO

Article history:
Received 2 May 2020
Received in revised form 7 September 2020
Accepted 18 September 2020
Available online xxxx
Editor: H. Handley

Keywords:
fulgurite
lightning
melting
paleoweather
Cascades
South Sister volcano

ABSTRACT

The process of meteorological lightning-induced modification of coherent volcanic rocks is examined by geochemical, textural, and experimental analysis of fulgurites from South Sister volcano, Oregon Cascades, USA. Lightning's effects on volcanic target rocks was simulated with an arc-welding device in order to reproduce the geochemical and textural features of natural fulgurites and to constrain temperatures of melting and devolatilization behavior during lightning strikes. Melting of volcanic target rocks produces melts of exceptional compositional diversity, ranging from those with pure mineral compositions (e.g., diopside and plagioclase), resulting from congruent melting reactions, to those that are highly mixed and compositionally identical to the target rock. Geochemical and textural observations on fulgurites suggest that melting proceeds rapidly, by an *in situ* modal batch process whereby individual crystals melt and contribute small aliquots to a larger batch that is then mixed by viscous flow. Hydrous species remaining in the glasses are trace ($OH \ll 0.1$ wt.%), and consistent with partial equilibration to high temperature (>2000 °C) supra-liquidus, 1-atm conditions. Lightning also induces physical weathering, in that the target rocks may be vapourized to form channels through the rock, representing injection of elemental components to the atmosphere. Finally, lightning acts as a multi-faceted producer of dry, chemically equivalent volcanic glass, which may be subject to long-term hydration by environmental waters at surface conditions. These re-hydration signatures contrast those of volcanic glasses, which have both magmatic and meteoric components, and are used herein to examine the post-lightning environmental history of these glasses, including age dating lightning events by diffusion chronometry. Our study of volcanic fulgurites illustrates the potential to use their hydration signatures to date paleoweather events at decadal to centuries scale. Because the lightning strike is in and of itself so effective at devolatilizing melts in an instant, the resultant fulgurites are a unique earth material that record individual weather events (i.e., a thunderstorm), and also longer-term paleoweather intervals.

> "*The presence of a porous rock, upon a prominent, acutely pointed mountain-summit in a region of violent electric storms presents the most favorable condition for the formation of fulgurite.*" –Diller (1884)

1. Introduction

The Earth's atmosphere is a significant agent of weathering and erosion of volcanic peaks. Weathering, the "alteration of rocks by exogenic processes acting at the surface" (Holmes, 1920), instigates chemical and physical "responses of materials which were in equilibrium within the lithosphere" (Reiche, 1945). While typically slow, weathering processes may be punctuated by lightning, whose rapid heating can melt and vaporize targets. The consequence of lightning hitting rock is apparent in the products left behind—rock fulgurites—glassy remains of the quickly formed and then quenched melts (Fig. 1). Fulgurites are common on volcanic peaks, where thunderstorm activity is induced by orographic uplift. The physicochemical effects of these rapid (~microseconds to 100 s of milliseconds; e.g., Uman, 1987; Rakov and Uman, 2003) melting events on coherent volcanic rocks atop peaks are not yet

* Corresponding author.
E-mail address: castroj@uni-mainz.de (J.M. Castro).

https://doi.org/10.1016/j.epsl.2020.116595
0012-821X/

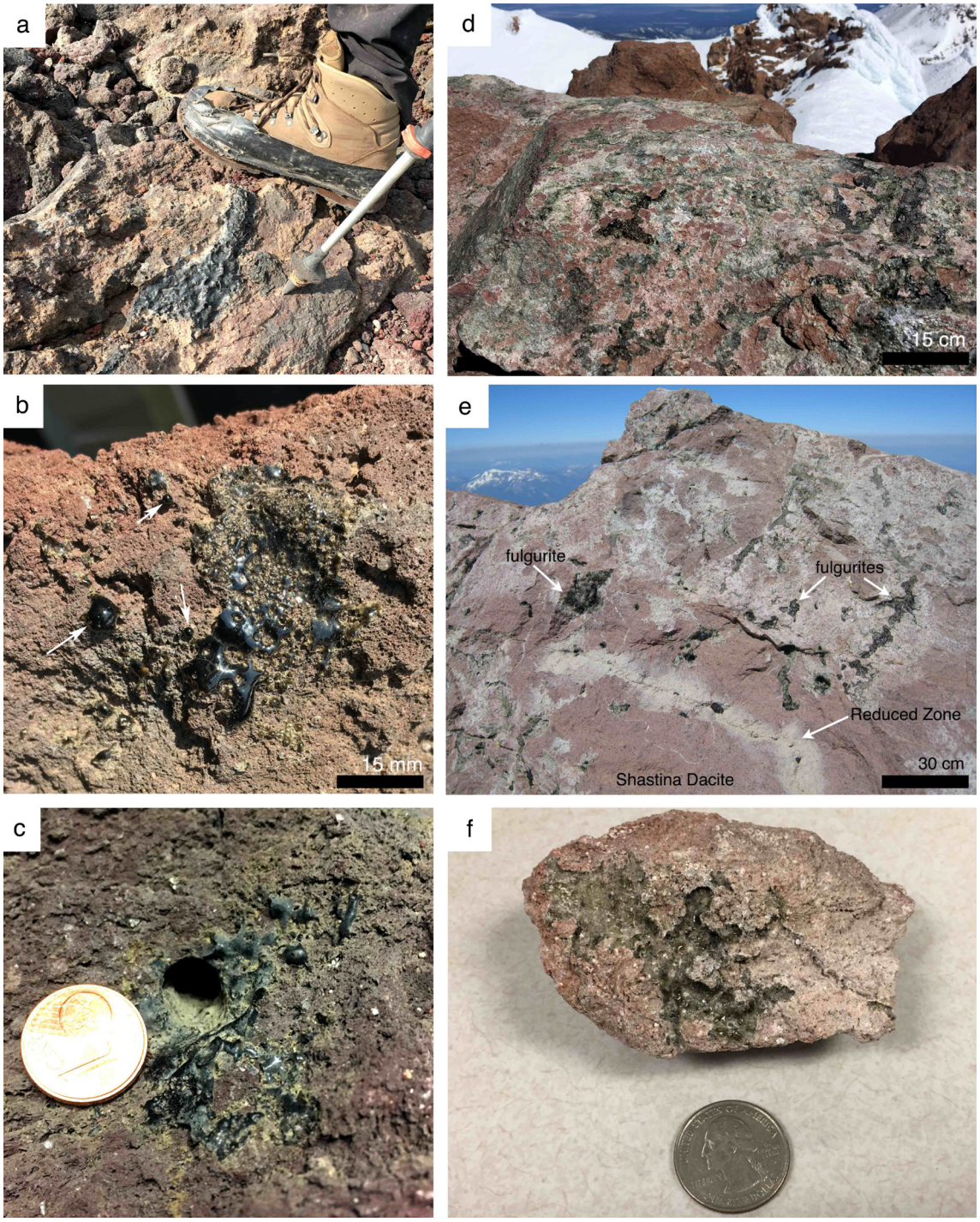

Fig. 1. Field occurrences of fulgurites atop Cascade volcanic peaks. a-c) Fulgurites from South Sister Volcano in basaltic andesite lava; d-f) fulgurites in Shastina dacite, CA. a) This example shows strong, *in-situ* melting evidenced by a thick (~1 mm) rind of dark grey glass. b) Superficial fulgurite "splash" form in basaltic andesite scoria. Here lightning formed an impact structure distributed over an area of several square centimeters and representing the source of several droplets of pure glass (white arrows). The droplets may have been ejected from the center of the impact structure. c) Close up of a fulgurite channel in South Sister lava. These features are characterized by a smooth glassy bore, some 0.5 to 1 cm in diameter and extending to depths of up to 15 centimeters in the target rock. d) Pervasive fulgurite pavements in dacite on Shastina, CA (photo by Chad Thomas). Light-pink dacite is the un-affected target rock. e) Fulgurite zones range from dark green though lime-colored and cover ~60% of the rock, forming hollow tubes and channels in the rock surface. The lighter color of host rock (note "Reduced Zone") mirrors the geometry of the fulgurite channels and may reflect local iron reduction during the lightning strike (e.g., Roberts et al., 2019). f) Hand sample of Shasta fulgurite showing completely aphyric glass and anastomosing trough structures comprising channels of negative relief. (For interpretation of the colors in the figure(s), the reader is referred to the web version of this article.)

thoroughly constrained (e.g., Wakasa et al., 2012; Roberts et al., 2019), and thusly, we examine the physical and chemical changes that occur during meteorological lightning-volcanic rock interaction.

Here we present field, analytical, and experimental evidence of profound changes in volcanic rock during lightning interaction on two Cascade volcanic peaks (South Sister and Mt Shasta). We then present experiments that reproduce all of the geochemical and textural features of natural fulgurites. Our findings highlight lightning's unique ability to melt rock, resulting in diverse geochemical patterns and near complete liberation of volatile elements into the atmosphere. The concentrations and distribution of H_2O remaining

in the fulgurite glasses record both high-T processes and subsequent low-T environmental rehydration. We develop these data into a new chronological tool to estimate the age of paleolightning events and longer-term paleoweather intervals with decadal to century resolution.

2. Background

Hundreds of thousands of lightning flashes occur on Earth each day, with cloud-to-ground lightning happening at the rate of about 10 strikes per second (Orville et al., 2011). The energy of these strikes is immense (up to $\sim 10^9$ Joules; J) and the temperature of the atmosphere may reach 30,000 K (e.g., Cooray, 2015). Evidence of rock and sediment melting indicates that the lightning fuses and vaporizes the solid substrate, which implies temperatures of several thousand of degrees (e.g., Pasek and Hurst, 2016).

Volcanic peaks force air upward and create favorable conditions for atmospheric convection (e.g., Banta, 1990; Rorig and Ferguson, 1999). In addition, owing to their elevation and relative proximity to cloud bases, mountain peaks promote step leader formation by shortening the distance between cloud base and target (Banta, 1990). Consequently, volcanoes see high amounts of lightning. The Cascades volcanic province—comprising some 20 Holocene to Paleocene volcanoes beginning in northern California (Sutter Buttes) and extending to southern British Columbia (Mount Meager)—receives on average 15-20 cloud-to-ground lightning strikes per 100 km^2 per year (van Wagtendonk and Cayan, 2008). Many of these strikes are concentrated on the volcanic peaks, between 2000-3000 m elevation (van Wagtendonk and Cayan, 2008). These average numbers belie the intense lightning activity that may occur during single thunderstorms, which can produce several hundreds to thousands of strikes daily (NWCC, 2019). Despite the Cascade peaks being well known for high lightning incidence—Mount Thielson carries the informal moniker "The Lightning Rod of the Cascades"—only cursory details of their fulgurites exist (Purdom, 1966; Switzer and Melson, 1972).

Fulgurites are glassy rocks that may form in either sediments (e.g., soils and sand) or on solid rock (e.g., Grapes and Müller-Sigmund, 2010). Most previous work has focused on sediment-hosted fulgurites, particularly in quartz sand whose compositions are simple ($\sim$90-99% SiO_2; e.g., Pasek et al., 2012). Such studies have elucidated the probable energy distribution of the lightning strikes themselves (Pasek and Hurst, 2016).

The formation conditions of fulgurites in polymineralic volcanic rocks are different from those of quartz-dominated sediments. For example, the resultant melts should have compositions that vary with the target mineralogy and the degree of melting (Switzer and Melson, 1972). Detailed geochemical analyses have been made on lightning-struck andesite from Little Ararat, eastern Turkey (Switzer and Melson, 1972), illustrating extreme major element heterogeneity over small distances (100 s of µms). Such compositional diversity apparently arises from isochemical melting of individual mineral grains and arrested admixing of these components in the bulk melts. Additional effects—to date untested—are the changes in fulgurites' hydrous species concentrations and long-term reaction in the weathering environment. We are not aware of prior work on these effects and therefore make it a goal to constrain the changes in fulgurites' major and minor element chemistry and texture due to lightning and later environmental exposure.

3. Samples and methods

3.1. Samples

Volcanic-rock hosted fulgurites ranging in mass from tens of grams to a few kilograms were carefully hammered out of outcrops on the summits of South Sister Volcano (Or) and Mount Shastina (Ca) during field campaigns from 2007 to 2019 (Fig. 1). Some of these samples served as the basis for textural and chemical characterization of natural fulgurites, while others—specifically selected from South Sister volcano—provided material for arcing experiments and detailed hydrous geochemical measurements. All sample sites comprise lava flows and domes of varying age (late Holocene; Brophy and Dreher, 2000; Christiansen et al., 1977) and these range from basaltic andesite (South Sister) to dacite (Shastina). The South Sister samples are lava fragments mantling the northwest summit. These rocks come from unit "PSba" of Brophy and Dreher (2000), which is equivalent to unit "mtp" of Fierstein et al. (2011), who determined an eruption age of $\sim$22.3 ka. The porphyritic basaltic andesites contain plagioclase (plag) and clinopyroxene (cpx), and minor orthopyroxene (opx) and olivine (ol) phenocrysts in a matrix comprising plag, cpx, Fe-Ti oxides, and interstitial glass (Fig. 1–3). It was impossible to ascertain whether the fulgurites formed recently or if they resulted from single or multiple lightning strikes. However, as hydrous geochemical data will show, all South Sister fulgurites are weakly hydrated, indicating sufficient time had passed for their uptake of meteoric water.

3.2. Experimental procedures

Electrical arcing experiments designed to generate a rapid heating pulse (e.g., Mueller et al., 2018) were performed to constrain the geochemical and textural effects of lightning-volcanic rock interaction. We used a modified form of an arc-welder configured by Mueller et al. (2018) to investigate the effects of rapid melting on volcanic rock cylinders (South Sister Basaltic Andesite). The device, "Electro Melt Simulator" (EMS) is an Oerlikon TIG arc welder (model CITOTIG DC 400), configured with two vertically opposed electrodes in a glass housing (Supplementary Information; Fig. S1). The EMS generates an electric arc in an Ar-purged chamber (Fig. S1). Maximum currents achievable with the EMS are 400 Ampere (A), but our experiments were limited to 50 A, which was guided by studies on volcanic ash (Mueller et al., 2018; Keller, 2018). Note, these current conditions are well below those of natural lightning ($\sim$30 kA for negative polarity, and up to 300 kA for positive polarity flashes; e.g., Uman, 1987), and consequently, the EMS does not simulate the electrical current impulse produced during natural lightning, as has been done in other studies (e.g., Genareau et al., 2019). However, the EMS does impose a sudden heating pulse on the rock, which permits investigation of the response of silicate rock targets to electrification events. EMS experiment conditions yielded estimated maximum plasma temperatures of 10,000 K (Bott, 1966), which are on the lower end of the range of temperatures ($\sim$10,000-28,000 K) achieved by natural lightning (Paxton et al., 1986).

In order to generate the electric arc, high-frequency, high-voltage electron sparks are emitted by the cathode (top of chamber), creating a conductive channel between the electrodes. As soon as the conductive channel arises, a plasma is created by charge separation, enhancing the electric field between the electrodes and thereby causing an arc, which is very much analogous to the high-intensity backstroke in cloud-to-ground lightning. The electric arcs were manually triggered and maintained at constant current for 200-300 milliseconds (e.g., Rakov and Uman, 2003), using a microprocessor that allowed for precise adjustment of arcing times. The EMS's arcing times resulted in significant melting of the samples (Fig. 2).

The experimental samples comprise cylindrical South Sister basaltic andesite cores approximately 1.36 cm in diameter by $\sim$1 cm thick (Fig. 2, S1). These cylinders were drilled out of slab-sawn hand samples with a diamond bore. The center of the cores were then bored with a 2 mm drill bit, which provided a path for the

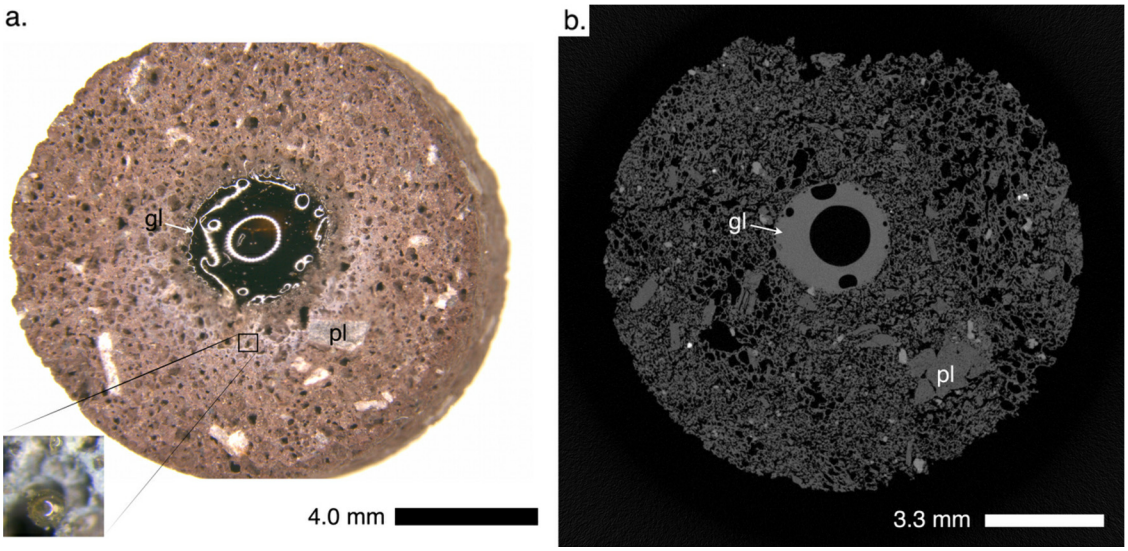

Fig. 2. a-b) Products of fulgurite experiments, in binocular optical view (a) and as a single image slice collected by an μ-Xray-CT scanner (b). The samples represent two separate experiments run at similar conditions (50 A; 230 ms). In each case, a zone of pure glass (gl) has formed at the center of the plagioclase (pl)-rich basaltic andesite sample, corresponding to the hot, high-energy plasma arc created by the EMS. These central glass domains contain large bubbles at their borders (note the black ellipsoids in μ-Xray image), a sign that the newly formed melt was hydrous and vesiculating as heating proceeded. Visible discoloration (white to light brown; frame a) of the target rock matrix occurred next to the glass, and within this zone, abundant tiny glass spherules are found (~20-300 μm), which likely formed during the melting event and their forceful ejection (see inset photo).

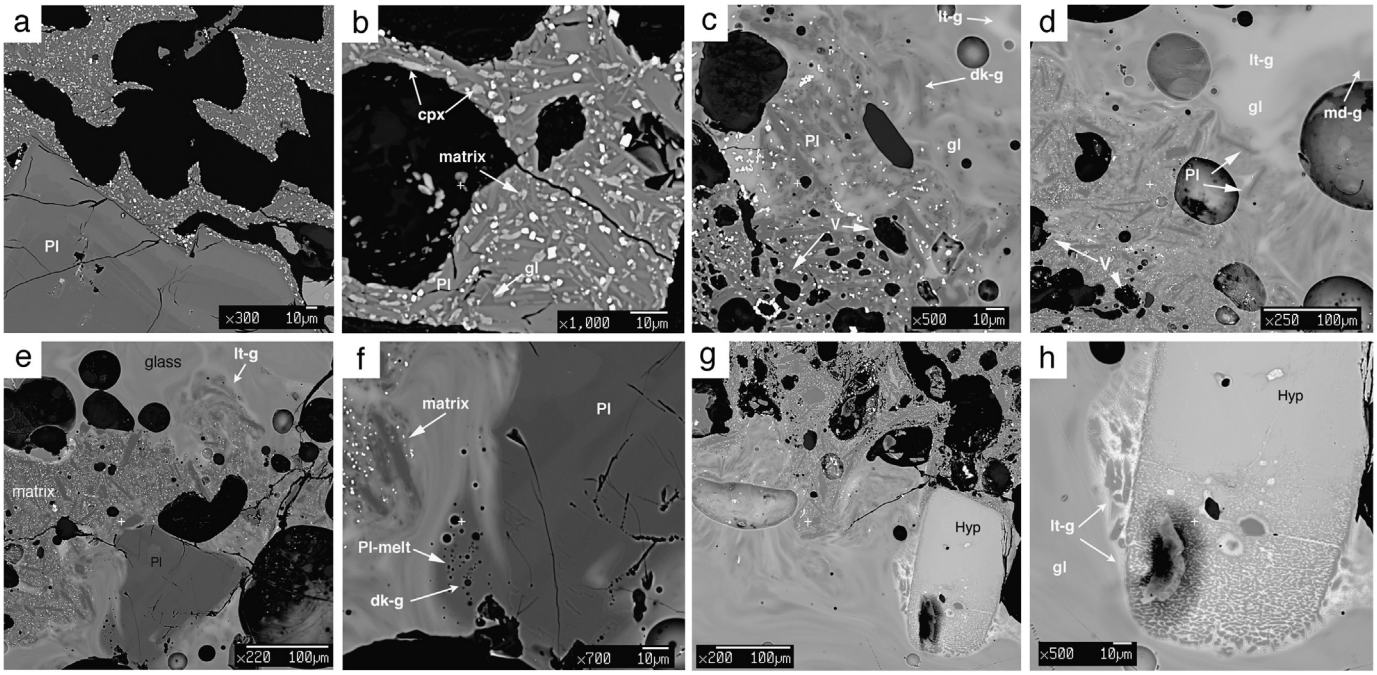

Fig. 3. BSE photomicrographs of pristine (a, b) lava textures and fulgurites (c-h) in South Sister basaltic andesite. Frames a) and b) show characteristic plagioclase (pl)-dominated phenocryst and groundmass (matrix) mineral populations, but also indicate an abundance of pyroxene (augite; cpx) and Fe-Ti oxide (ox) in the matrix. The highly crystalline matrix also contains ~5% bubble-free interstitial glass (gl; frame b). Images c) and d) show the contact zone between pristine matrix (lower left) and fulgurite glass (upper right). These transition zones are characterized by partially melted microlites (pl) and small (≤10 μm) round vesicles (V) in the glass and between matrix-dwelling microlites. Such textures are evidence of incipient melting and frothing of the matrix. Further away from the interface, ghost-like blobs of plagioclase form dark glass domains (dk-g). Fulgurite glass is relatively homogenized farthest from the transition zone represented by light- and mid-grey glasses (lt-g and md-g; upper right in frames c and d). Frames e) and f) show a partially melted plagioclase phenocryst with a microvesicular dark glass melt domain attached to its host crystal (f). The small vesicles in the dark blob confirm that the plagioclase was completely and congruently molten. Images g) and h) indicate partial melting of an orthopyroxene (hypersthene; $En_{62}Fs_{35}Wo_7$) microphenocryst. Unlike the plagioclase (e,f), this pyroxene appears to have melted incongruently, as evidenced by its mottled appearance.

arc pass through. Owing to the voltage limits of the EMS, it was not possible to generate an arc that propagated through solid rock, hence the bore was used to instigate melting reactions between the arc and rock. Each experiment involved positioning a rock disk on a glass cylinder between the two electrodes and then triggering an arc. As a result, the plasma arc melted the samples, resulting in a greenish-black glass interior that enlarged center bore by about 1 to 2 mms (Fig. 2, S1).

Sample temperature was measured at two positions using a Voltcraft infrared thermometer (IR 1200-50D USB; T_{max}=1200 °C) and an Optris CS laser thermometer (T_{max}=1600 °C). Both devices are accurate to ± 1 °C, and record temperature with time (sam-

pling at 1/10th of a second). The Voltcraft infrared thermometer was aimed side-on, to the outer surface of the sample (recording relatively modest T<100 °C), while the Optris device was pointed at the top side of the cylinder, close to the discharge channel (Fig. S1). The Optris laser thermometer, being close to the arc, detected much higher temperatures (T>1600 °C) than the Voltcraft device, and always "clipped" due to high temperature (IR) overload of the sensor (Supplementary Information). Because the Optris' T-time measurements yielded continuous curves showing an exponential heating ramp, a plateau (due to clipping), and an exponential cooling ramp, we were able to estimate the minimum melting temperatures near the discharge channel by fitting the heating and cooling segments with regression curves, and then extrapolating these regressions to an intersection point above the temperature plateau. These methods yielded minimum T estimates of∼1900 °C, which is consistent with the approximate melting points of silicate phases observed in experimental and natural fulgurites (Supplementary Information).

3.3. Sample preparation and analytical techniques

Natural and experimental samples were cleaned, sectioned with a diamond saw, and embedded in epoxy. The epoxy-bound fulgurites were then exposed by sawing and ground flat and polished with diamond lap wheels. The polished sections were then subjected to various analyses: Scanning Electron Microscopy (SEM), Electron Probe Microanalysis (EPMA), and Fourier Transform Infrared Spectroscopy (μ-FTIR). Electron microbeam imaging (BSE mode) was performed on a 5-spectrometer JEOL Superprobe, using 10-12 nA beam currents with a scanning 3-µm beam, while quantitative wavelength dispersive X-Ray analysis was performed with an acceleration voltage of 15 keV, 10 nA current, and beam diameters ranging from defocused (10 µm; glass) to focused (2 µm; minerals). Quantitative X-Ray element maps were made following the routine of Lanari et al. (2019), which uses an internal standardization method involving spot analyses of standards (along with ZAF corrections) for accurate determination of X-Ray intensities while accounting for a continuum background. Each sample was mapped with a 2 µm beam, 15 keV, 100 nA current, and dwell times of 180 ms. X-Ray intensities were measured by WDS (Mg, Na, Mn, Al, K) and EDS (Si, Ti, Fe, Ca, Cr). Data reduction was performed using XMapTools software (v. 2.5.2; Lanari et al., 2014).

Remnant H_2O in the fulgurite glass was quantified by μ-FTIR using a Thermo-Nicolet FTIR Bench with attached Continuum microscope. Doubly polished wafers (∼400-900 µm) were analyzed on aperture constrained spots (∼25-50 µm) in transmission mode at a spectral resolution of 4 cm^{-1}, 256 scans, and with sample-free-path background spectra collected every 30 minutes. The very thick samples promoted quantifiable mid-IR absorbance peaks, resulting in good signal-to-noise and low detection limits. We estimate detection limits of ∼0.005 wt.% H_2O based on the repeat analysis of the 3550 cm^{-1} peak and observing consistency as we collected unknown sample spectra at various scan numbers.

We also made FTIR line maps using Omnic Mapping Software. In these cases we applied variable step sizes (10-25 µm) to capture compostional detail. Despite the samples' large thickness, and thus long IR-beam-path lengths, the only peak with a suitably strong signal was the bulk "water" peak ∼3550 cm^{-1} representing the fundamental O-H stretching vibrations in both molecular H_2O and SiOH and AlOH groups (e.g., Mandeville et al., 2002). We therefore used this band's peak height along with a linear baseline to determine absorbance values that would then be input into Beer's Law for quantification. We used extinction coefficients appropriate for basaltic andesite glass (70.3 L/mol/cm^{-1}, King et al., 2002; 61.4 L/mol/cm^{-1}, Mandeville et al., 2002). We calculated glass densities using the major element compositions and the approach of Lange and Carmichael (1990). In addition to microanalytical measurements, we also measured the bulk composition of the South Sister basaltic andesite by X-Ray Fluorescence using a MagiXPRO-XRF instrument.

4. Results

4.1. Structural, textural, and microscopic features of natural fulgurites

Fulgurites at the tops of Cascade Peaks comprise a variety of forms (Fig. 1; Diller, 1884; Switzer and Melson, 1972). The most abundant is a skin-like glassy veneer (1-5 mm thick) covering several square cms of the rock's surface (Figs. 1a, d). The dark-green to brown color of these fulgurites distinguishes them from the relatively lighter color of the host. Another morphology is a "splash" form (Fig. 1b), so-called because these comprise roughly circular, crater-like depressions filled with vesicular glass. The edges of these features contain adhered droplets of black glass (<1 mm to > 1 cm), and reminiscent of ejecta strewn about an impact crater (Fig. 1b). The most distinctive morphology are glass-lined tubes (3-6 mm in diameter) that penetrate the rock up to 15 cm or alternatively may manifest trough-like forms in the rock surface (Fig. 1). In one example from South Sister, a nearly perfectly straight bore, some 0.5 cm in diameter extends through the rock (Fig. 1c). The opening of the bore is surrounded by glass apron whereas the other end bifurcates into anastomosing tubes. Similar tube fulgurites were described by Switzer and Melson (1972) in hornfels on Castle Peak, Co, and in andesite from Little Mount Ararat, Turkey. These workers concluded that such tubes form on the timescale of the lightning strike—in just milliseconds—and indicate that the rock was completely vaporized. What is clear from these field relations is that the fulgurite formation generates new porosity (Fig. 1), yet also densifies previously vesicular and partially weathered volcanic target rock.

4.2. Experimental fulgurite formation

Tests of the EMS on un-drilled rock cylinders indicated failure of arc formation, due to blockage by the sample itself. However, experiments on pre-drilled samples, along with arc-pulse durations (200-300 ms) that overlap with long-duration natural lightning strikes (Essene and Fisher, 1986; Rakov and Uman, 2003) resulted in significant melting of the rock (Fig. 2). We estimated minimum melting temperatures of ∼1900 °C based on thermal IR temperature measurements (Supplementary Information). These T-estimates are consistent with *in situ* melting of various silicate mineral phases (e.g., Deer et al., 1992).

Experimental glasses preserve many microtextural and geochemical features that are virtually indistinguishable from those in nature (Figs. 2–5). Glassy domains, comprising brown glass at the sample center, vary from slightly larger than the original bore (∼2 mm) to many times greater (>6 mm), indicating significant enlargement of the bore during melting (Fig. 2). Some melt was ejected from the bore during melting, as evidenced by abundant small (50-250 µm) glass droplets nested in pores within the unaltered matrix (Fig. 2a inset). These droplets are akin to those seen in natural fulgurites (Fig. 1b).

Experimental fulgurites are devoid of crystals, except for what appear to be incipiently melted phenocrysts and groundmass crystals at the margins of the glass where it contacts the matrix (Fig. 2). Glass-matrix boundaries (Fig. 2b) are always vesicular, indicating bubble growth during melting. Microscopic observations—to be discussed in further detail in section 4.3—show that some matrix appears to have also vesiculated as it contains small (<10 µm) vesicles in the interstices between microlites (Fig. 2, 5).

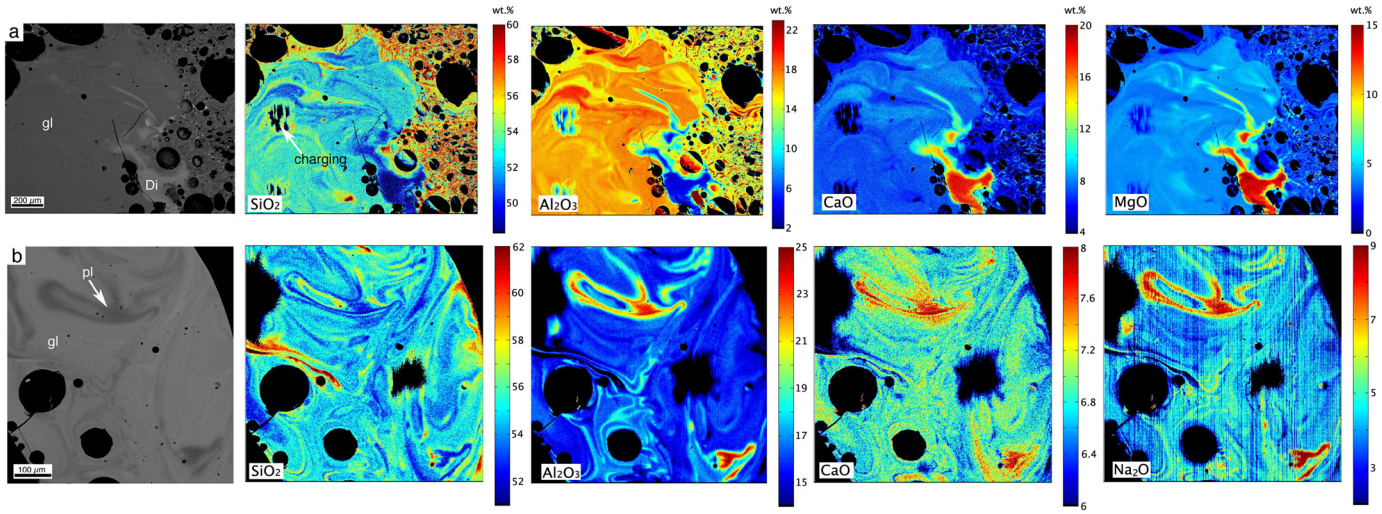

Fig. 4. BSE photomicrographs (at left) and major element EPMA maps showing compositional variability in natural fulgurite glass. Each colored frame represents the 2D distribution of a given major-element oxide, our selection of which demonstrates the most dramatic yet small-scale compositional chemical variations that arise from the rapid melting event. Notable in row (a) is an incipiently melted Diopside crystal (di), whose CaO and MgO content stand out in stark contrast to the surrounding matrix and moderately well mixed fulgurite glass. In row (b), we find a loop-shaped plagioclase melt with wispy filament extensions demarcated by very high Al_2O_3, CaO, and Na_2O relative to background levels in the host glass. The preservation of very fine compositional filaments indicates the brevity of the melting, mingling, and quenching event, as all three of these processes precluded diffusive equilibration of the sharp concentration gradients. Note that the vertical lines in the Na_2O frame are related to charging effects during scan acquisition.

This indicates that the matrix was actively degassing. The geochemical aspects of these phases will be discussed in the next section.

4.3. Major and element compositional trends, mineral melting and mixing

4.3.1. Natural fulgurite glass (melt) classification

Here we classify natural fulgurites according to their glass geochemistry and compare their compositions to the South Sister Basaltic Andesite (e.g., Brophy and Dreher, 2000; Fig. 3, 4; Supplementary Figure S6).

BSE images and compositional maps of natural fulgurites are shown in Figs. 3–4, and quantitative EPMA data of the natural glasses are given in Table 1. Although much of the glass appears medium grey in BSE mode (Fig. 3), close examination reveals heterogeneity, comprising light and dark mingled glass filaments (Fig. 3g, 4). These structures represent mixing of crystal- and matrix-derived melts (Fig. 3, 4). The matrix-derived glasses—those directly in contact with matrix—are variable in BSE intensity, which appears to manifest contributions from groundmass phases (plag, cpx, and Fe-Ti oxide) to the melt (Fig. 3; Supplementary Figure S6). Matrix melts exhibit slight major element differences from the target bulk-rock composition (Supplementary Figure S6; Table 1).

We group glasses into three categories based on BSE intensity (Fig. 3; Table 1); these are termed “dark-”, “mid-”, and “light-grey” glasses. The mid-grey glass is volumetrically most abundant (∼50-90%), and is a near one-to-one match for the bulk-rock composition (Table 1). The dark-grey glass occurs almost exclusively in contact with incipiently melted plagioclase crystals and matrix domains that feed larger pools of mid-grey glass (Fig. 3c and 3f). This glass is the most aluminous with high CaO and Na_2O and very low FeO, MgO and TiO_2 (Fig. 4). The light-grey glasses are the most compositionally diverse, having varied yet low SiO_2 and high ferromagnesian components (Table 1). Light grey glasses occur in direct contact with ferromagnesian minerals (e.g., hypersthene; Fig. 3h; diopside; Fig. 4a), but also form diffuse filaments that appear to emanate from Fe-Ti oxides in the melting area (Fig. 3g; Supplementary Figure S6).

4.3.2. Experimental fulgurite glasses

Experimental glasses resemble the natural glasses, and like them, show exceptional textural and compositional diversity (Fig. 5; Table 1). These contain filament structures near matrix-melt contact (Fig. 5a), and also vesicles at the border between glass and un-melted matrix (Fig. 5b). As before, we group experimental glasses into light-, mid- and dark-grey varieties (Table 1). Figs. 5a and b show the representative glass types and in particular the abundance of the mid-grey component out board of the matrix-melt contacts (Fig. 5).

Experimental glasses closely resemble the respective natural glass compositions (Table 1), with mid-grey glasses being identical to the natural mid-grey glass, as well as the bulk rock (Table 1). The dark-grey glasses show slightly higher FeO and MgO contents than the natural dark glasses, however all other major elements are identical. Finally, the light-grey glasses are not as chemically diverse as the natural light glasses (Table 1), but the low SiO_2 and high ferromagnesian components are consistent with the natural equivalents.

The origin of diverse experimental glasses—and by extension the natural ones—can be gleaned by comparing mineral phases to adjacent fulgurite glass compositions (Figs. 5c-f). For example, EPMA spots measured in a dark-grey glass blob emanating from the tip of a melted plagioclase microphenocryst (An_{50}) shows a nearly one-to-one correspondence between the glass and plagioclase composition (Fig. 5d). This confirms that dark melt was sourced from the plagioclase crystals. Light-grey glass appears to accumulate in pools near oxide-rich matrix domains (Fig. 5a), or as selvages adjacent to olivine and pyroxene (Fig. 5e). These glasses do not show a one-to-one correspondence with any specific mineral (Fig. 5f), but rather appear to have been mixed into the neighboring mid- and/or dark-grey melts. Finally, we find no correspondence between mid-grey glass a specific mineral. These glasses are thoroughly mixed and are compositional equivalents of the bulk rock. In summary, geochemical observations indicate that lightning (or arc melting) produces homogenized glasses that manifest the natural rock’s bulk composition.

Table 1
Average major element composition of South Sister Basaltic Andesite and natural and experimental fulgurites.

Bulk Rock[1]													
	SiO_2	TiO_2	Al_2O_3	FeO	MnO	MgO	CaO	Na_2O	K_2O	Cl	F	Total	LOI
Major Element Oxide (wt.%)	55.6	1.26	17.7	8.00	0.14	4.17	7.70	4.14	0.98	n.d.	n.d.	100.70	1.03
Representative Minerals[1]													
Plagioclase (n=5)	56.7	0.06	26.4	0.59	0.01	0.07	9.66	5.93	0.36	0.001	0.057	99.82	
Orthopyroxene (n=6)	52.3	0.23	0.72	22.1	0.75	22.7	1.48	0.06	0.72	0.004	0.000	100.35	
Fe-Ti Oxide (n=2)	0.1	16.3	2.36	71.0	0.18	2.52	0.05	0.00	0.00	0.015	0.000	92.48	
Olivine (n=5)	39.6	0.02	0.04	20.4	0.30	41.2	0.19	0.01	0.00	0.005	0.000	101.84	
Natural fulgurites[2]													
	SiO_2	TiO_2	Al_2O_3	FeO	MnO	MgO	CaO	Na_2O	K_2O	Cl	F	Total	
Dark grey (n=34)	56.9	0.08	26.4	0.68	0.01	0.13	9.46	6.01	0.34	0.006	0.019	100.01	
Mid-grey (n=156)	56.2	1.32	17.7	8.0	0.14	3.88	7.41	4.35	1.01	0.006	0.014	100.01	
Light-grey_1 (n=3)	35.9	7.51	10.5	33.8	0.26	4.17	4.30	2.97	0.66	0.004	0.000	100.00	
Light-grey_2 (n=3)	48.5	3.38	14.7	17.1	0.19	4.42	7.32	3.60	0.79	0.006	0.004	100.00	
Light-grey_3 (n=3)	54.6	1.40	13.5	12.2	0.24	6.53	6.53	4.00	0.97	0.007	0.009	100.01	
Average all light-grey	48.4	3.42	13.0	18.8	0.23	5.41	6.17	3.64	0.84	0.006	0.006	100.00	
									Ave. Halogens	**0.006**	**0.009**		
Standard deviation of respective melts													
1-σ dark	1.2	0.06	0.9	0.41	0.01	0.21	0.75	0.36	0.15	0.009	0.015		
1-σ mid	1.4	0.14	1.3	0.68	0.03	0.59	0.72	0.66	0.22	0.005	0.015		
1-σ all light	8.1	2.62	2.5	9.34	0.07	2.49	1.31	0.69	0.21	0.006	0.011		
Experimental fulgurites[2]													
	SiO_2	TiO_2	Al_2O_3	FeO	MnO	MgO	CaO	Na_2O	K_2O	Cl	F	Total	
Dark grey (n=8)	55.3	0.24	26.2	1.86	0.03	0.58	9.92	5.40	0.51	0.004	0.023	100.01	
Mid-grey (n=18)	56.2	1.30	17.8	7.84	0.14	3.95	7.14	4.47	1.07	0.006	0.011	100.01	
Light-grey (n=10)	52.2	1.81	13.2	12.2	0.26	6.11	9.92	3.55	0.72	0.009	0.033	100.02	
									Ave. Halogens	**0.006**	**0.023**		
Standard deviation of respective melts													
1-σ dark	2.3	0.27	3.2	1.72	0.042	0.91	2.18	0.72	0.42	0.005	0.020		
1-σ mid	1.5	0.21	1.9	0.80	0.028	1.09	1.13	0.44	0.16	0.005	0.014		
1-σ light	1.0	0.33	1.6	1.23	0.049	1.27	1.31	0.35	0.12	0.009	0.022		

[1] Determined by XRF.
[2] Determined by EPMA.

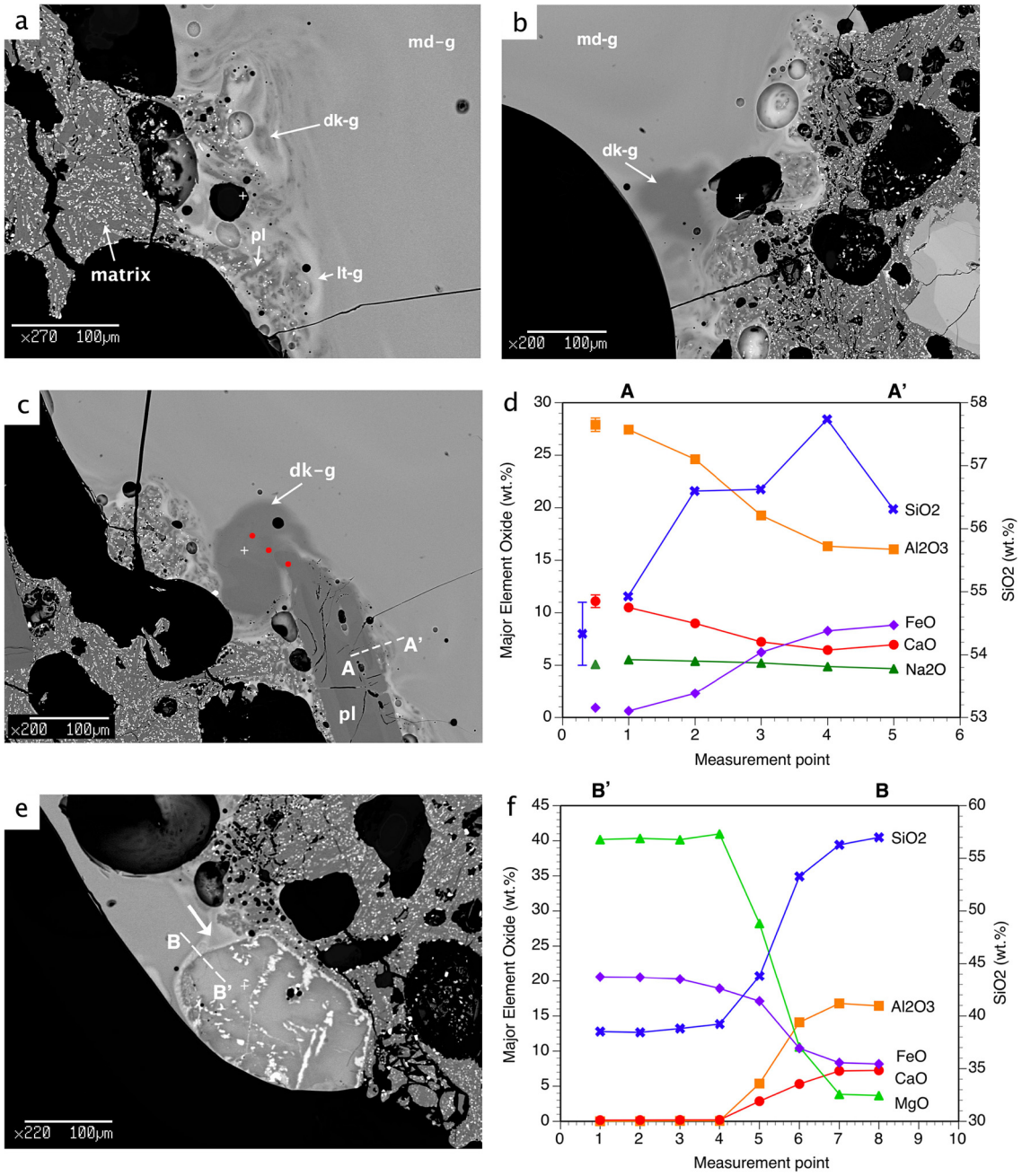

Fig. 5. Experimental fulgurite glasses imaged in BSE mode and analyzed by EPMA. Frames a) and b) show an abundance of mid-grey glass, a heterogeneous glass-matrix border zone, characterized by microfilaments of light, mid- and dark-grey glass, and vesicular textures likely originating from the heat pulse. The plagioclase microphenocryst (pl) in frame c) is connected to an irregular dark glass blob that appears to "flow" from the microphenocryst (dk-g). This texture indicates *in situ* melting of this individual crystal. EPMA analyses of this dark glass are shown in frame d), at the far left side, and represent an average of the three red spots shown in the dark blob in frame c). Despite some variation in composition, indicated by the error bars of 1 s.d., the dark glass is a nearly 1:1 match of major element chemistry of the plagioclase, the analysis of which is given by measurement point 1, or point "A" on the line traverse (A-A'). The relatively large variation in SiO_2 (~5 wt.%) in the dark glass is likely due to in-mixing of adjacent mid-grey melts as the crystal underwent rapid fusion. Frames e) and f) show a line traverse across an olivine phenocryst, indicating highly disparate crystal and glass compositions. In frame e), an olivine crystal (Fo_{63}) appears to build a small (~10 µm wide) light-grey glass selvage (indicated by arrow) of a very different composition to that of the olivine crystal, suggesting immediate in-mixing of the neighboring mid-grey melt and consequently shifting glass composition away from olivine.

4.4. Natural and experimental H_2O content distribution

FTIR measurements on natural fulgurite glasses, made on two separate samples and comprising four distinct line traverses (Fig. 6), indicate that bulk H_2O contents of the fulgurite are low (~0.04-0.07 wt.%), and unevenly distributed in the natural glass. The fulgurites' water content is hereafter referred as "OH concentration", to account for empirical evidence that silicate glasses are devoid of molecular H_2O at low total water contents (<0.2 wt.%; Stolper, 1982). The OH concentration distribution of natural fulgurites exhibits maximum values (~0.07 wt.%) at glass surfaces (Fig. 6). These surface OH-peaks, which we term "secondary" due to their probable meteoric origin (e.g., Anovitz et al., 2004), sharply decrease (~0.04-0.06 wt.%) over just tens of µm. OH concentration then fluctuates by minor amounts (<0.005 wt.%) to the glass-matrix boundaries (Fig. 6). However, as observed in two traverses (Fig. 6b, d), OH concentration again rises at the matrix-glass boundary, over ~200 µm. These peaks, which terminate in the vesicular zone of the glass-matrix boundary (Fig. 6b, c) are termed "primary" due to their close association with vesicles near

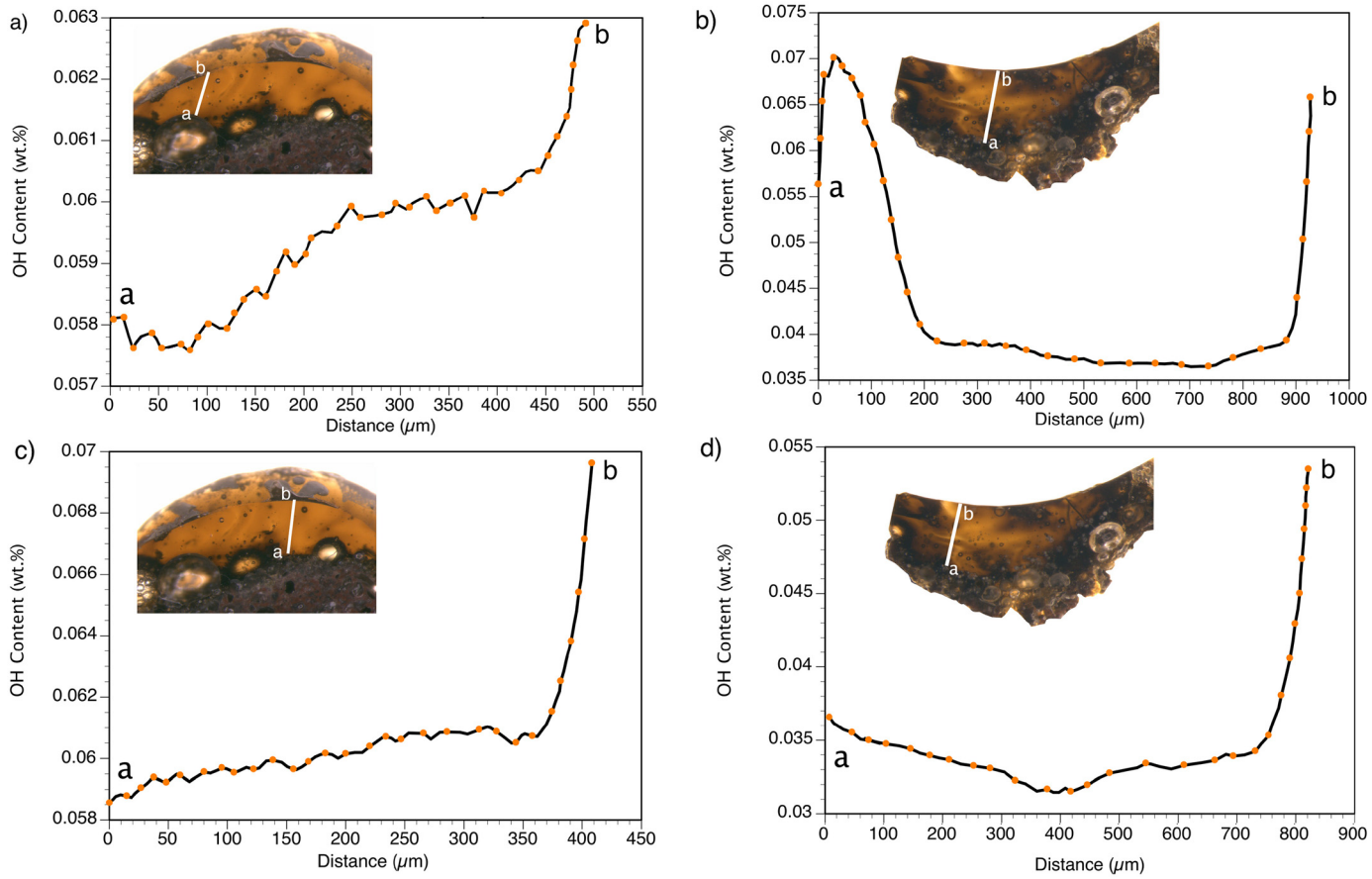

Fig. 6. FTIR profile measurements on two natural South Sister fulgurite samples indicating the OH concentration distribution along four separate linear traverses. Each frame's inset photomicrograph shows the measured sample and superimposed FTIR profile in bold white, with white letters indicating the corresponding start (a) and end (b) positions of the concentration profile. All profiles emanate from the vesicular interface between the rock matrix (reddish) and the pure fulgurite glass (light brown). In the case of the fulgurite in frames a) and c), OH content is minimal at the matrix interface and climbs steadily away, peaking sharply at the glass surface (note white "b"). The strong upturns at the glass surface, indicate incipient post-quench hydration due to interaction with meteoric water (secondary OH-peaks). These hydrated rinds penetrate to some ~30-50 μm within the sample. Similar secondary peaks are observed in the natural samples shown in frames b and d, however these also exhibit OH increases at the glass-matrix boarders, indicating remnant magmatic OH and post-lightning diffusion.

the melting front. The OH content of primary peaks reaches similar values as those observed at the glass surfaces, however, their broader extent and sigmoidal form (Fig. 6b) are distinguishing features.

The OH-concentration distributions of experimental fulgurite are shown in Fig. 7. These glasses have OH contents that overlap with the lower range of values observed in natural samples (~0.026-0.046 wt.%; Fig. 6). Like the natural fulgurites, OH-concentration reaches a "primary" maximum at the vesicular glass-matrix boundary (Fig. 7). These peaks decay over a couple hundred μm's, similar to the pattern in natural fulgurites (Fig. 6). However, in contrast to the natural fulgurite, the OH concentrations do not form secondary peaks.

5. Discussion

5.1. Major element modifications during lightning-induced melting

The microtextural and geochemical characteristics of fulgurites (e.g., Fig. 3–5; Table 1) are unique indicators of melting that occurs when lightning strikes volcanic rock. In essence, fulgurites' compositions (Table 1) record melt formation from matrix and individual phenocrysts, and the ensuing mixing that occurs (Fig. 5). Crystalline phases melted rapidly and *in situ*, and then they underwent variable mixing to form different melts. The melt affinities range from pure crystal (e.g., plagioclase) to mechanical mixtures of two or more different melts (light- and dark-grey melts), to completely homogenized melts identical to the bulk rock (mid-grey melt). The glasses produced by laboratory experiments confirm that natural glasses derive from different source materials, those being: 1) light-grey melts from Fe-Mg silicates and Fe-Ti oxides; 2) dark-grey melts derive from plagioclase; and 3) mid-grey melts from all sources resulting in a hybridized replica of the bulk rock. Thus, the most abundant mid-grey melts are arguably the "end-point" in lightning-induced fusion.

Melting conditions during lightning strikes differ significantly from magmatic environments in the following ways: 1) heating rates are extremely large (1000's °C in ms; e.g., Switzer and Melson, 1972; Pasek et al., 2012; Supplementary Information), and 2) heating occurs over very small length scales (μms-cms). Due to these factors lightning is capable of producing both highly diverse, and bulk-rock-equivalent melts in a small space and time (e.g., Fig. 5c). By contrast, melting in igneous environments (e.g., a volcanic arc), is likely slow, involving polymineralogic contributions to growing melt batches that collectively may never attain the composition of the original rock due to limited heat and low melting degrees (e.g., McBirney, 1992).

It is therefore remarkable that lightning makes bulk-rock equivalent melts with apparent ease. In order to build the abundant mid-grey melt, whose composition is nearly the same as the bulk rock (Table 1), efficient and rapid homogenization would have had to occur. This in turn requires vigorous mixing. Evidence for this

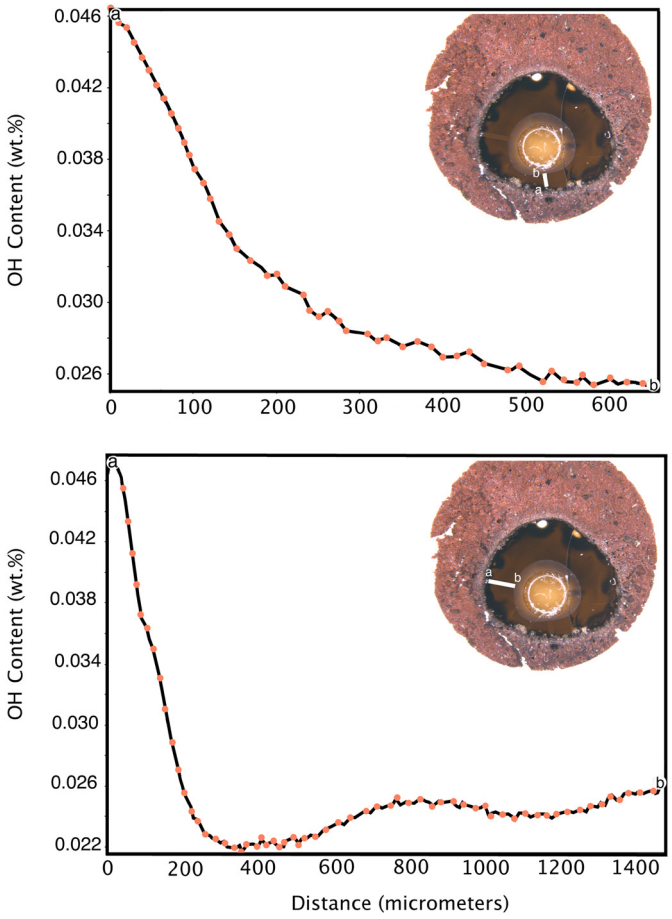

Fig. 7. H_2O content profiles (FTIR) on an experimental fulgurite (South Sister Basaltic Andesite). The inset photomicrographs show the sample measured with brown glass interior and surrounding unaltered rock matrix. The approximate positions of the measurement traverses are shown as bold white lines. The left hand side of each profile corresponds to the melt-matrix boundary and thus the most advanced stage of melt/glass formation. Both profiles exhibit very similar distributions of OH concentration, both in terms of absolute values and the manner in which OH content is at a maximum at the boundary and sharply decreases with distance from the interface. Slight differences in OH content in the distal edge of the profiles, corresponding to the former contact between melt and the arc itself, could reflect the effect of mixing of a vigorously flowing melt at the time of extreme heating.

includes high-speed videos of other EMS experiments (Mueller et al., 2018) showing that silicate melts are extremely fluid, with bubble oscillations providing significant driving force to mix the melt (Mueller et al., 2018). Vestiges of melt mixing include extremely elongate mineral-melt filaments emanating from the melt-matrix boundaries (Fig. 4), suggesting very large strains over millisecond timescales, and indicating that low melt viscosities were at play.

Melt viscosities (Table 1) can be estimated by the Giordano et al. (2008) model, assuming a temperature of ~2000 °C (Supplementary Information). This temperature is higher than Giordano et al.'s (2008) experimental calibration, and thus uncertainty exists with the following estimates. Such calculations yield melt viscosities for the light-, mid- and dark grey compositions: ~ 0.7 (dark), 0.23 (mid), and 0.05 Pa sec (light-grey), respectively. Given the possibility that natural lightning and experimental temperatures were higher, we consider these estimates to be maximum values. That said, these still represent exceedingly low viscosities, especially compared to volcanic melts (~10^4-10^{13} Pa sec^{-1}; e.g., Gonnermann and Manga, 2007). Low melt viscosity aided in rapid melt homogenization, which in turn would have fostered efficient outgassing of the melts.

5.2. Volatile component evolution during lightning strikes

Fulgurites in volcanic rocks are unique materials in which OH-concentrations and their spatial distributions record both high (~100 s to 1000 s of °C) and low temperature (10's of °C) processes. Hydrous geochemical signatures furthermore record events happening over highly disparate temporal scales, both the rapid lightning-induced melting of volcanic rocks, and the ensuing long-term exposure of the fulgurite glass at the earth's surface. Collectively these characteristics represent the ideal conditions for dating paleoweather events on volcanic mountains.

However, in order to make proper analysis of these highly disparate processes, the high (magmatic)- and low (meteoric)-temperature hydrous component signatures must be interpreted separately (e.g., Giachetti and Gonnermann, 2013). The next two sections address water (OH) contents of fulgurites, specifically their spatial variations manifested in the primary and secondary OH signatures in natural and experimental fulgurites.

FTIR measurements indicate that natural and artificial fulgurite glasses are depleted in H_2O (~0.02-0.07 wt.%; Figs. 8 and 9), especially in comparison to volcanic glass of eruptive origin (~0.1 to a few wt.%'s H_2O; Helo et al., 2011; Castro et al., 2014). While these low values could suggest that the original volcanic targets were almost completely degassed upon eruption, we contend that the lightning event "boiled off" most volatiles inherent to the original rock (e.g., Mueller et al., 2018). In addition to magmatic water, the target rock may have also contained some water stemming from low-T weathering at the surface; these hydrous components could be manifested in the ~1 wt.% LOI in XRF analyses (Table 1).

Several lines of evidence support rapid and thorough degassing of the target rock. Firstly, fulgurite glasses next to the glass-matrix boundary are vesicular, and vesicles are found nested in the interstitial glass just inboard of the matrix-glass boundary (Fig. 3c; 5b). Matrix farther afield from the glass-matrix boundary is nonvesicular. Thus, the border zone vesicles, and abundant large vesicles in the glass indicate that a boiling event, caused by lightning and driven by volatiles from the newly melted matrix had occurred.

Secondly, the low OH contents (~0.02-0.07 wt.%) are consistent with high-T degassing at surface (low-P) conditions. The expected bulk H_2O contents of these melts can be estimated with the Papale et al. (2006) volatile solubility model, with the caveat that this model's underlying dataset does not cover basaltic andesite compositions at 1-atm pressure. We thusly view the estimates to be order-of-magnitude. Such calculations indicate melt-H_2O contents of ~0.030 wt.% at 750 °C and ~0.005 wt.% at 2250 °C (Supplementary Information). These values are comparable to the H_2O contents in natural and experimental fulgurites (~0.02-0.07 wt.%). Consequently, the fulgurites' OH concentrations reflect near-equilibration to atmospheric conditions. To our knowledge, such low total H_2O contents have only been rarely observed in volcanic obsidians and tektites (e.g., Gilchrist et al., 1969).

Thirdly, the primary OH gradients (Fig. 6, 7) indicate that hydrous components were not spatially equilibrated before being quenched. In particular, the primary OH profiles comprise a peak value near the glass-matrix boundary that then decays over ~100's of μm, suggesting that H_2O was diffusing from the matrix boundary zone to a drier, quite possibly hotter molten zone in closer proximity to the electric arc and/or natural lightning strike. Indeed, the OH-concentration profiles (Fig. 7) at the glass-matrix interfaces have exponential forms characteristic of diffusion from high to low chemical potential (e.g., Castro et al., 2005, 2008; Feisel et al., 2019). We can estimate the timescales over which H_2O diffusion occurred by numerically fitting OH concentration data with solutions to 1D chemical diffusion equations (e.g., Castro et al., 2005, 2008; Supplementary Information). We assume that OH-concentration curves were the result of instantaneous melt de-

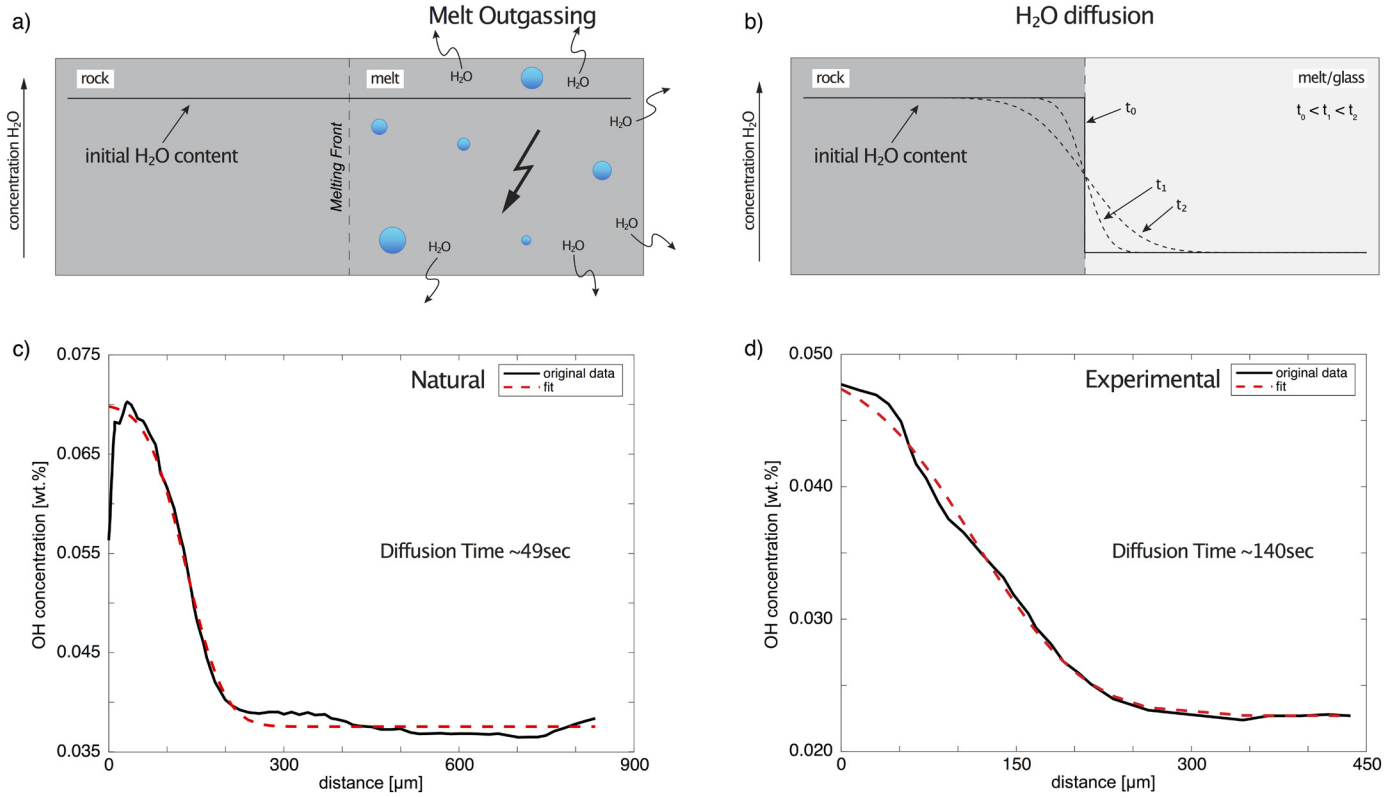

Fig. 8. a, b) Schematic diagrams showing a simplified model of magmatic OH-concentration profile development. In a), the target rock half-space is struck by lightning (z-shaped bold arrow), resulting in melting, boiling (bubbles in blue) and instantaneous outgassing to low levels (see concentration curve, frame b RHS). A melting front propagates to the left at this time, creating relatively cooler melt having more dissolved H_2O that was taken up by actively melted matrix. b) During the lightning strike and for a period of time after, the relatively wetter melt at LHS diffusively releases its water to the dry RHS, resulting in a concentration profile. Primary OH peaks are in this case interpreted to be the vestiges of water-loaded melts next to an actively melting matrix, that in turn lend their water to relatively drier far-field melt. Hence a step-function change in OH concentration at t=0 will evolve with time (b). Within the context of this simple physical model (a,b), we show best-fit solutions to the 1D diffusion equation (T=2000 °C) to observed OH concentration data measured on c) natural and d) experimental primary OH profiles (d). Best fit diffusion times range from seconds to minutes. See supplementary material for further explanation.

hydration followed by diffusion from the adjacent matrix, which was supplying H_2O to the dehydrated melt (Fig. 8). This procedure considers the water-enriched melt-matrix boundary as a half space that feeds H_2O into the depleted melt (Fig. 8b). Subsequent cooling from high temperature, buffered perhaps by the lingering heat of the lightning strike, may have allowed OH-concentration distributions to further develop. However, this complexity cannot be captured with our model, which is kept simple in order to achieve an order-of-magnitude estimate. Boundary and initial conditions are: 1) constant T∼2000 °C; 2) maximum and minimum OH values are from the analytical traverses (Figs. 6, 7), and 3) a constant H_2O diffusivity equal to the expression given in Zhang and Behrens (2000).

Diffusion model fits to natural and experimental primary OH profiles yield timescales on the order of several tens of seconds to minutes (Figs. 8c, d). We consider these diffusion model fits to be first-order measures of the melting event and cooling history of the fulgurite samples. Best-fit time scales would shorten and lengthen, respectively, if temperatures were to be increased or decreased. However, given the uncertainties surrounding cooling history of the melt, we hesitate to further investigate scenarios that lack constraints on the thermal histories of fulgurites. In nature, lightning parameters (e.g., energy and duration) do vary widely (e.g., Uman, 1987; Pasek and Hurst, 2016), and we expect this variability to translate to diverse forms of primary OH profiles. The assumption here being that shapes of OH profiles should become more evolved (protracted H_2O diffusion will "flatten" the curves) with increasing thermal energy, that would in turn buffer the cooling of the glass. This highlights the potential to use primary OH profiles as qualitative measures of the intensity of lightning strike. When coupled with estimates of the cooling history of glass (e.g., DSC geospeedometry; e.g., Nichols et al., 2009) primary OH profiles could help quantitatively track the strength of multiple lightning strikes during weather timescale events (e.g., paleo-thunderstorms; Yan et al., 2020). While our dataset does not allow us to assess this idea, we nevertheless consider the diffusion model estimates as *maximum* times of the protracted H_2O diffusion interval that followed a rapid melting pulse, indicating relatively short lived (∼1 min) melting and cooling events.

Thus far, our analyses indicate that lightning causes residual H_2O to be rapidly taken up into the newly formed melt, and eventually outgassed as the melt vesiculates. The heat of the lightning strike drives rapid volatile exsolution and vesiculation (Figs. 2 and 3; e.g., Mueller et al., 2018), rendering the glass effectively dry in fractions of a second. The resultant dry glasses are in turn the perfect template for low-T weathering, including glass hydration.

5.3. Post-lightning glass hydration

As demonstrated in the previous section, lightning produces very dry glasses. These glasses, once exposed to the elements, will slowly hydrate. The natural fulgurite samples demonstrate this, as OH-profiles evidence meteoric water uptake by the glass during environmental weathering (Fig. 6).

Fulgurites on volcanoes have been exposed to surface waters for variable, yet unknown durations. Owing to their exceptional degrees of dehydration by lightning, these glasses contain negligible magmatic water, and any water added to their surface dur-

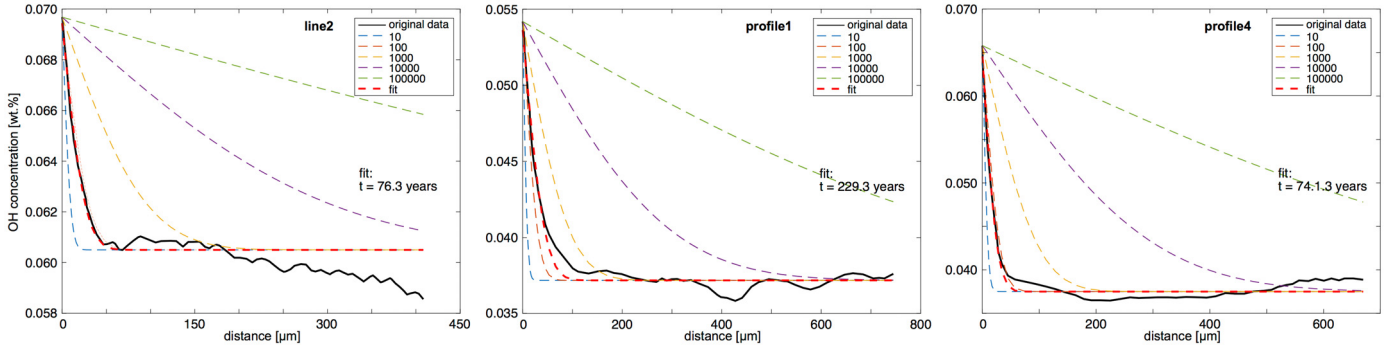

Fig. 9. Best-fit model solutions to the diffusion-sorption equation in Cartesian coordinates on natural fulgurite secondary OH-concentration (wt.%) vs. position (µm) data. Frames a, b, and c show measurement traverses made on different surfaces of a single fulgurite glass sample. Colored dashed curves are model solutions for different times, shown in hours in the upper right hand side legend box. These model fits suggest that the fulgurite-forming lightning event happened several decades to centuries ago.

ing weathering will be meteoric. This assumes that the fulgurites have not been altered by later hydrothermal or volcanic outgassing activity. These high-T processes could enhance hydration and corrode the glass. However the South Sister fulgurites appear to be unaltered and exceptionally dry, and we contend that they have not been subject to high-T processes since formation. We therefore propose that once fulgurites begin rehydrating, they will act as records of the low-T, H_2O-rich surface environment, which in turn may permit reconstruction of past weather. Thus, fulgurites fall into a unique category of earth material that may record individual events (i.e., an electrical storm), but also longer-term surface weathering, after the lightning. In this section we demonstrate that even subtle levels of post-melting hydration offers quantitative insights into when lightning struck rock.

Fulgurites exhibit a secondary OH-maximum at the glass surface where it would have been exposed to the environment (Fig. 6). These OH gradients are absent from the experimental glasses (Fig. 7)—these glasses had no exposure to water since formation—thus, the natural OH signatures reflect hydration during exposure to surface waters post-lightning. While the amount of OH upturn at the surfaces indicates minor enhancement in OH concentration above the "far field" values (~10-70%), the width over which this takes place is relatively constant (~50 µm), indicating relatively uniform uptake of H_2O. We interpret these OH-patterns as hydration rinds, similar to those observed on volcanic obsidians and used to age date artifacts (Friedman et al., 1966).

Obsidian rind dating involves measuring the width of a hydration rind and, assuming hydration proceeded at a constant rate, determining age by multiplying rind width by a rate estimate (e.g., Friedman and Smith, 1960; Friedman and Long, 1976). However, due to the tediously slow rates of hydration of glass (e.g., Anovitz et al., 2004), experimentally constrained hydration rates at surface weathering conditions (<20 °C) are nonexistent, rendering age estimates from this method highly uncertain. Published hydration rates derive from experiments performed at elevated temperatures (75-245 °C; Friedman and Long, 1976; Anovitz et al., 2004), or from diffusion modeling of glass hydration patterns (Seligman et al., 2016). Both methods yield a wide range of rates extrapolated to surface temperatures (~1-10 µm/1000 yrs). Applying these rates to the South Sister hydration rinds (~50 µm) yields ages on the order of thousands of years (~5-50 kyr), which in some cases exceed the age of the lavas themselves (~23.2 ka; Fierstein et al., 2011).

An alternative approach is to use an H_2O diffusion model to fit the measured OH-position data. To this end, we numerically solved the 1D equation for sorption of H_2O into a semi-infinite solid medium for variable times (Fig. 9; Zhang, 2010, eq. 42; Supplementary Information):

$$C = C_s + (C_i - C_s) * \mathrm{erf}\left(\frac{x}{\sqrt{4Dt}}\right)$$

where C_s is the surface concentration of the fluid, C_i is the initial fluid concentration in the glass, t is time in seconds, D is the diffusion coefficient in m^2/s and x is the distance from the interface in meters. The term *erf* is the error function. The diffusion coefficient D was calculated using equation 14 of Zhang and Behrens (2000), based on high-T experiments (T>Tg). However, a complication in using the Zhang and Behrens (2000) model for extrapolating diffusivities to low T (20 °C) is that the values do not match existing low-T empirical data (e.g., Anovitz et al., 2008; cf. Fig. 3), but rather are offset to much slower D. Thus, we corrected the diffusion coefficients calculated with Zhang and Behrens (2000) by factors of 10^5 to 10^6 in order to account for the diffusivity discrepancies between high- and low-T data (e.g., see Fig. 3 of Anovitz et al., 2008). We chose C_s and C_i values to match to the measured OH-contents at the surface and in the far field respectively. Where the OH fluctuated in the far field, we chose an average value that best represented a constant OH concentration (Supplementary Information).

The best-fit diffusion-equation solutions (with D correction of 10^5) to three secondary hydration profiles (Fig. 9) in natural fulgurites indicate times of decades (~70 yrs) to centuries (~230 yrs). Time estimates are reduced by an order of magnitude when a D correction factor of 10^6 is used, suggesting that hydration times could be as short as about 1 decade to several decades (Fig. 9). Clearly, model diffusion times depend sensitively on D, and since this factor is not known *a priori*, D uncertainty could result in under- (D erroneously fast) and overestimating (D erroneously slow) lightning age.

Uncertainty notwithstanding, the best-fit hydration times provide order of magnitude dates, i.e., ~10^1-10^2 yrs, representing both the age of lightning strike and the ensuing exposure time of the glasses undergoing surface weathering. Natural hydration rates could also be variable, stemming from different H_2O diffusion rates whose variability depends on humidity and fluids' access to fulgurite. Nevertheless, the decadal- to century-scale dates seem consistent with the fulgurites' subtle hydration amounts and steep OH-profile geometry (Fig. 9a-c), and most importantly, these dates are significantly shorter than those from the hydration rind method. Fulgurite dates are furthermore viewed as *minimum* lightning ages, as glasses made in significantly younger lightning events would either not be hydrated to any appreciable extent (e.g., Anovitz et al., 2008) or, where subtly hydrated, would require more precise measurement techniques (e.g., synchrotron FTIR; Castro et al., 2005) to constrain trace uptake of OH on the glass surface.

In summary, the decades- to centuries-old lightning age on South Sister volcano constitutes a proof-of-concept that fulgurite analysis could enable paleoweather dating on volcanic peaks and other mountainous environments prone to lightning strikes (Diller, 1884). The first such paleoweather date of its kind, the age of

this fulgurite-producing lightning strike at South Sister demonstrates that even minor amounts of hydration can be measured and modeled to yield decadal to centennial age information about the weather events that produce them. This is possible because lightning produces dry glass from inception by driving off residual magmatic H_2O in the host rock. Typical volcanic glasses always contain primary magmatic H_2O (~0.1-3.0 wt.%; e.g., von Aulock et al., 2014), which may mute hydration gradients, rendering age estimates difficult, unless steps are taken to "unmix" hydration and magmatic signatures (e.g., Seligman et al. 2016).

Our modeling approach, when applied to a broader set of samples, from multiple peaks, could reveal a range of hydration amounts and by extension, lightning ages. Indeed, preliminary diffusion models run at very long times yield evolved OH profiles with distinct exponential forms (e.g., 10^3 and 10^4 year models, Fig. 9) that could be used to fit the potential OH signatures of natural fulgurites that have been hydrated over long timescales. This could in turn permit paleoweather analysis of volcanic peaks over protracted intervals (~tens of millennia), at a temporal resolution not previously achieved. Fulgurite dates could also be used to interpret the ages of glacial moraines perched high on the volcanic peaks, provided these have been struck by lightning. Glacial advances on volcanic peaks are manifested by moraines, and are key in reconstructing past climate fluctuations in alpine settings (Marcott et al., 2009). However relative and stratigraphic methods (e.g., geomorphic relations; tephrochronology), and absolute dating techniques (e.g., cosmogenic nuclides; Nishiizumi et al., 1992) have large uncertainties (centuries to millennia). Finally, fulgurite age dates could provide initial reconnaissance ages of the volcanic deposits (eruptions) on which they form, which in conjunction with other methods may chronicle past volcanic activity.

6. Conclusions

A lightning strike on a volcanic peak represents a unique event that produces distinct evidence (fulgurite glass) ideal for analysis of paleoweather events and surface processes over extended geological time periods. We have shown that lightning does three things when it strikes volcanic rocks: 1) instant and rapid melting of the rock to produce mineral melts plus volumetrically dominant bulk-rock melts; 2) dries out the rock by liberating remnant H_2O, thereby providing an exceptionally dry glass that will then be prone to secondary hydration and, 3) sets a geochemical "clock" for determining the timing of the lightning event by hydration rind diffusion chronometry. We conclude that the best targets for analyzing ancient weather conditions on volcanic peaks are the very glasses produced by those events, whose rapid formation primes them chemically and physically for the uptake of environmental waters. Fulgurites may be age dated, which in turn could be the basis for paleoenvironment analyses with decade-to-century scale resolution.

CRediT authorship contribution statement

J.M. Castro conceived of the project, collected samples and data, and co-wrote the manuscript. All co-authors contributed equally to data collection and interpretation and aided in co-writing the manuscript.

Declaration of competing interest

The authors declare that they have no known competing financial interests or personal relationships that could have appeared to influence the work reported in this paper.

Acknowledgements

This work was supported by the VAMOS research center at the Johannes Gutenberg University, Mainz. The authors thank Steve Anderson and Hugh Tuffen for assistance in the field. The authors are grateful for the comments of two anonymous reviewers and the careful handling of the manuscript by the editor, Dr. Heather Handley.

Appendix A. Supplementary material

Supplementary material related to this article can be found online at https://doi.org/10.1016/j.epsl.2020.116595.

References

Anovitz, L.M., Elam, J.M., Riciputi, L.R., Cole, D.R., 2004. Isothermal time-series determination of the rate of diffusion of water in Pachuca obsidian. Archaeometry 46, 301–326.
Anovitz, L.M., Cole, D.R., Fayek, M., 2008. Mechanisms of rhyolite glass hydration below the glass transition. Am. Mineral. 93, 1166–1178.
Banta, R.M., 1990. The role of mountain flows in making clouds. In: Blumen, W. (Ed.), Atmospheric Processes over Complex Terrain. In: Meteorological Monographs, vol. 23. American Meteorological Society, Boston, MA, pp. 229–283.
Bott, J.F., 1966. Spectroscopic measurement of temperatures in an argon plasma arc. Phys. Fluids 9 (8), 1540–1547.
Brophy, J.G., Dreher, S.T., 2000. The origin of composition gaps at South Sister volcano, central Oregon: implications for fractional crystallization processes beheath active calc-alkaline volcanoes. J. Volcanol. Geotherm. Res. 102, 287–307.
Castro, J.M., Manga, M., Martin, M.C., 2005. Vesiculation rates of obsidian domes inferred from H_2O concentration profiles. Geophys. Res. Lett. 32, L21307.
Castro, J.M., Beck, P., Tuffen, H., Nichols, A.R.L., Dingwell, D.B., Martin, M., 2008. Timescales of spherulite crystallization in obsidian inferred from water concentration profiles. Am. Mineral. 93, 1816–1822.
Castro, J.M., Bindeman, I.N., Tuffen, H., Schipper, C.I., 2014. Explosive origin of silicic lava: textural and δD-H_2O evidence for pyroclastic degassing during rhyolite effusion. Earth Planet. Sci. Lett. 405, 52–61.
Christiansen, R.L., Kleinhampl, F.J., Blakely, R.J., Tuchek, E.T., Johnson, F.L., Conyac, M.D., 1977. Resource appraisal of the Mt. Shasta wilderness study area, Siskiyou, County, California. Open-file Report 77-250. Geological Survey, US. 102 pp.
Cooray, V., 2015. An Introduction to Lightning. Springer Verlag, pp. 97–116.
Deer, W.A., Howie, R.A., Zussman, J., 1992. An Introduction to the Rock Forming Minerals, 2nd edition. Longman Scientific & Technical. 696 pp.
Diller, J.S., 1884. Fulgurite from Mount Thielson, Oregon. Am. J. Sci. 28, 252–258.
Essene, E.J., Fisher, D.C., 1986. Lightning strike fusion: extreme reduction and metal-silicate liquid immiscibility. Science 234 (4773), 189–193.
Fierstein, J., Hildreth, W., Calvert, A.T., 2011. Eruptive history of South Sister, Oregon Cascades. J. Volcanol. Geotherm. Res. 207, 145–179.
Feisel, Y., Castro, J.M., Dingwell, D.B., 2019. Diffusion of F and Cl in dry rhyodactic melt. Am. Mineral. 104, 1689–1699.
Friedman, I., Smith, R.L., 1960. A new method of dating using obsidian: part I, the development of the method. Am. Antiq. 25, 476–522.
Friedman, I., Smith, R.L., Long, W.D., 1966. Hydration of natural glasses and formation of perlite. Geol. Soc. Am. Bull. 77, 323–328.
Friedman, I., Long, W., 1976. Hydration rate of obsidian. Science 191, 347–352.
Genareau, K., Wallace, K.L., Gharghabi, P., Gafford, J., 2019. Lightning effects on the grain size distribution of volcanic ash. Geophys. Res. Lett. 46 (6), 3133–3141.
Giachetti, T., Gonnermann, H.M., 2013. Water in volcanic pyroclast: rehydration or incomplete degassing? Earth Planet. Sci. Lett. 369–370, 317–332.
Gilchrist, J., Thorpe, A.N., Senftle, F.E., 1969. Infrared analysis of water in tektites and other glasses. J. Geophys. Res. 74, 1475–1483.
Giordano, D., Russell, J.K., Dingwell, D.B., 2008. Viscosity of magmatic liquids: a model. Earth Planet. Sci. Lett. 271, 123–134.
Gonnermann, H.M., Manga, M., 2007. Fluid mechanics inside a volcano. Annu. Rev. Fluid Mech. 39, 321–356.
Grapes, R.H., Müller-Sigmund, H., 2010. Lightning-strike fusion of gabbro and formation of magnetite-bearing fulgurite, Cornone di Blumone, Adamello, Western Alps, Italy. Mineral. Petrol. 99, 67–74.
Helo, C., Longpré, M.-A., Shimizu, N., Clague, D.A., Stix, J., 2011. Explosive eruptions at mid-ocean ridges driven by CO_2-rich magmas. Nat. Geosci. 4, 260–263.
Holmes, A., 1920. The Nomenclature of Petrology, 1st ed. Thos Murby, London, van Nostrand, New York. 284 pp.
Keller, F., 2018. Alteration of volcanic rock and plume chemistry by lightning. M.Sc. Thesis. University of Mainz, Germany. 96 pages.
King, P.L., Vennemann, T.W., Holloway, J.R., Hervig, R.L., Lowenstern, J.B., Forneris, J.F., 2002. Analytical techniques for volatiles: a case study using intermediate (andesitic) glasses. Am. Mineral. 87, 1077–1089.

Lange, R.A., Carmichael, I.S.E., 1990. Thermodynamic properties of silicate liquids with emphasis on density, thermal expansion and compressibility. In: Russell, J.K., Nicholls, J. (Eds.), Modern Methods of Igneous Petrology; Understanding Magmatic Processes. In: Reviews in Mineralogy, vol. 24, pp. 25–64.

Lanari, P., Vidal, O., De Andrade, V., Dubacq, B., Lewin, E., Grosch, E.G., Schwartz, S., 2014. XMapTools: a MATLAB©-based program for electron microprobe X-ray image processing and geothermobarometry. Comput. Geosci. 62, 227–240.

Lanari, P., Vho, A., Bovay, T., Airaghi, L., Centrella, S., 2019. Quantitative compositional mapping of mineral phases by electron probe micro-analyser. In: Ferrero, S., Lanari, P., Goncalves, P., Grosch, E.G. (Eds.), Metamorphic Geology: Microscale to Mountain Belts. In: Geological Society of London, Special Publications, vol. 478, pp. 39–63.

Mandeville, C.W., Webster, J.D., Rutherford, M.J., Taylor, B.E., Timbal, A., Faure, K., 2002. Determination of molar absorptivities for infrared absorption bands of H_2O in andesitic glasses. Am. Mineral. 87, 813–821.

Marcott, S.A., Fountain, A.G., O'Connor, J.E., Sniffen, P.J., Dethier, D.P., 2009. A latest Pleistocene and Holocene glacial history and paleoclimate reconstruction at Three Sisters and Broken Top Volcanoes, Oregon, U.S.A. Quat. Res. 71, 181–189.

McBirney, A., 1992. Igneous Petrology, 2nd ed. Jones and Bartlett Publishing Inc. 508 pp.

Mueller, S.P., Helo, C., Keller, F., Taddeucci, J., Castro, J.M., 2018. First experimental observations on melting and chemical modification of volcanic ash during lightning interaction. Sci. Rep. 8 (1389), 1–9.

Nichols, A.R.L., Potuzak, M., Dingwell, D.B., 2009. Cooling rates of basaltic hyaloclastites and pillow lava glasses from the HSDP2 drill core. Geochim. Cosmochim. Acta 73, 1052–1066.

Nishiizumi, K., Kohl, C.P., Arnold, J.R., Dorn, R., Klein, J., Fink, D., Middleton, R., Lal, D., 1992. Role of in situ cosmogenic nuclides ^{10}Be and ^{26}Al in the study of diverse geomorphic processes. Earth Surf. Process. Landf. 18, 407–425.

NWCC, 2019. Northwest annual fire report 2019. Northwest Interagency Coordination Center, Portland, Oregon. 43 pp.

Orville, R.E., Huffines, G.R., Burrows, W.R., Cummins, K.L., 2011. The North American lightning detection network (NALDN)—analysis of flash data: 2001-2009. Mon. Weather Rev. 139, 1305–1322.

Papale, P., Moretti, R., Barbato, D., 2006. The compositional dependence of the saturation surface of H_2O + CO_2 fluids in silicate melts. Chem. Geol. 229, 78–95.

Pasek, M.A., Block, K., Pasek, V., 2012. Fulgurite morphology: a classification scheme and clues to formation. Contrib. Mineral. Petrol. 164, 477–492.

Pasek, M.A., Hurst, M., 2016. A fossilized energy distribution of lightning. Sci. Rep. 6, 30586. https://doi.org/10.1038/srep30586.

Paxton, A.H., Gardener, R.L., Baker, L., 1986. Lightning return stroke. A numerical calculation of optical radiation. Phys. Fluids 29, 2736.

Purdom, W.B., 1966. Fulgurites from Mount Thielsen. Ore Bin 28 (9).

Rakov, V.A., Uman, M.A., 2003. Lightning: Physics and Effects. Cambridge University Press, New York. 687 pp.

Reiche, P., 1945. A Survey of Weathering Processes and Products. University of New Mexico Publications in Geology, no. 1. University of New Mexico Press. Albuquerque, 87 pp.

Roberts, S.E., Sheffer, A.A., McCanta, M.C., Dyar, M.D., Sklute, E.C., 2019. Oxidation state of iron in fulgurites and trinitite: implications for redox changes during abrupt high-temperature and pressure events. Geochim. Cosmochim. Acta 266, 332–350.

Rorig, M., Ferguson, S.A., 1999. Characteristics of lightning and wildland fire ignition in the Pacific Northwest. J. Appl. Meteorol. 38, 1565–1575.

Stolper, E., 1982. Water in silicate glasses: an infrared spectroscopic study. Contrib. Mineral. Petrol. 81, 1–17.

Switzer, G., Melson, W., 1972. Origin and composition of rock fulgurite glass. Earth Sci. 9.

Uman, M.A., 1987. The lightning discharge. Int. Geophys. 39, 188–204.

van Wagtendonk, J.W., Cayan, D.R., 2008. Temporal and spatial distribution of lightning strikes in California in relation to large-scale weather patterns. Fire Ecol. 4 (1), 34–55.

von Aulock, F.W., Kennedy, B.M., Schipper, C.I., Castro, J.M., Martin, D.E., Oze, C., Watkins, J.M., Wallace, P.J., Puskar, L., Bégué, F., Nichols, A.R.L., Tuffen, H., 2014. Advances in Fourier transform infrared spectroscopy of natural glasses: from sample preparation to data analysis. Lithos 206–207, 52–64.

Wakasa, S.A., Nishimura, S., Shimizu, H., Matsukura, Y., 2012. Does lightning destroy rocks?: results from a laboratory experiment using an impulse high-current generator. Geomorphology 161, 110–114.

Yan, H., et al., 2020. Extreme weather events recorded by daily to hourly resolution biogeochemical proxies of marine giant clam shells. Proc. Natl. Acad. Sci. USA 117 (13), 7038–7043.

Zhang, Y., 2010. Diffusion in minerals and melts: theoretical background. In: Zhang, Y., Cherniak, D.J. (Eds.), Reviews in Mineralogy, vol. 72, pp. 311–408.

Zhang, Y., Behrens, H., 2000. H_2O diffusion in rhyolitic melts and glasses. Chem. Geol. 169, 243–262.